Article

Modeling of Electrical Machines Hysteresis Losses Under Mechanical Stresses

Indiara P. C. da Silva[1] , Rodrigo A. Miranda[1] , Nelson Sadowski[1] , Nelson J. Batistela[1] ,
Laurent D. Bernard[1] , João Pedro A. Bastos[1,2,3]

[1] Postgraduate program in electrical engineering (PPGEEL), GRUCAD, UFSC, Florianópolis, SC, Brazil.
indiara.pitta@posgrad.ufsc.br, rodrigo.miranda@posgrad.ufsc.br, nelson.sadowski@ufsc.br,
jhoe.batistela@ufsc.br, laurent.bernard@ufsc.br, assumpcao.bastos@ufsc.br
[2] Postgraduate program in electronic systems (PPGESE), UFSC, Joinville, SC, Brazil.
[3] Postgraduate program in power systems (PPGSE), UTFPR, Curitiba, PR, Brazil.

Abstract— **The effect of mechanical stress on hysteresis losses of electrical steel sheets is investigated in this paper. Experimental data obtained from a dedicated bench are used in a curve fitting procedure to analyze the parameters behavior for a hysteresis losses model over a range of mechanical compressive and tensile stresses. By applying the concept of equivalent stress, a finite element model is simulated, and the hysteresis losses are a posteriori calculated considering an equivalent stress distribution over a single-phase induction motor stator.**

Index Terms—Electrical Machines, Finite Element Method, Hysteresis Losses, Magneto-mechanical coupling.

I. INTRODUCTION

Electrical machines can be subjected to different mechanical stresses, such as the mechanical load that comes from shrink-fitting procedures for stators, the mechanical stress that appears in rotors due to centrifugal forces at high-speed and from manufacturing procedures as electrical steel sheets cutting and stamping.

To evaluate the behavior of electromagnetic devices considering mechanical loads, different approaches can be applied, including robust predictive multiscale models [1] and simplified formulations [2], [3]. The last approaches are particularly interesting when evaluating losses in post-processing Finite Element (FE) field calculations because they are less expensive in computation aspects.

For this purpose, several low frequency tests involving different levels of mechanical stresses and samples cut according to different orientations with respect to lamination directions were performed.

After analyzing several approaches considering different tensile and compression mechanical stresses, a formulation intended to reproduce the behavior of the iron sheet sample losses is chosen.

The main contributions of this work are related to a very deep and exhaustive experimental research on the evaluation of the behavior of hysteresis losses on samples of industrial applied electrical iron sheets. This research provides a losses calculation formulation considering the different mechanical

loads levels applied to samples cut on different directions with respect to the lamination directions. A generic equation is proposed in order to obtain the evolution of the parameters of the model according to stress values. It allows the use of the here obtained experimental data in other works focused on the evolution of losses in electromagnetic devices.

The proposed model is finally applied to the evaluation of losses on a real stator core of a single-phase induction motor under mechanical stress. In this modeling, hysteresis losses are a posteriori calculated considering an equivalent stress distribution. It shows the expected influence of the complex stress distribution on the local and global losses.

II. MATERIAL AND METHODS

To precisely quantify the impact of mechanical stresses on the magnetic thin steel sheets properties, an experimental bench is used (Fig. 1); it is designed to match international standards established for magnetic measurements [4]. A PWM power inverter with a LC low pass filter is used to generate the magnetic excitation on a Single Sheet Tester (SST), in addition to a nonlinear closed-loop control based on the sliding modes theory and implemented with analog circuits. Such a system allows the generation of an excitation signal so that the induced voltage on the secondary winding of the magnetic circuit corresponds to a defined reference, chosen to be sinusoidal in this paper. The frequency used is 1 Hz for neglecting dynamic losses. The mechanical loads are applied by employing a tester machine (MECMESIN®), which allows the generation of loadings up to 2500 N. An anti-buckling fixture was designed to avoid bending of steel sheets under compressive stress and is highlighted in Fig. 1 [4].
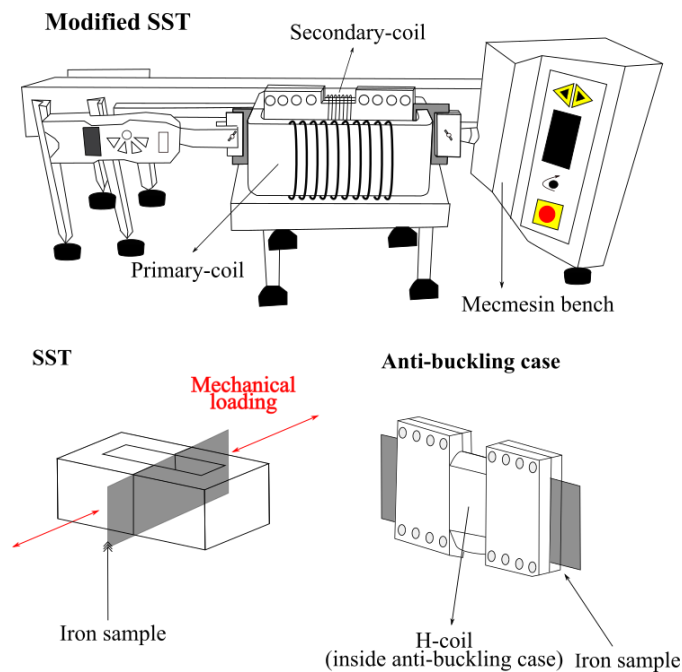

Fig. 1. Magneto-mechanical bench (Modified SST) with emphasis on the SST and the anti-buckling case.

A. Testing Methodology

For the experimental procedure, non-oriented 0.5 mm thickness steel sheet samples cut along the rolling (RD), transversal (TD) and diagonal (DD) directions are used.

The influence of mechanical stresses on the magnetic characteristics of the material is considered using the σ-H methodology. This way, a constant mechanical stress value σ is applied, followed by the imposition of different magnetic excitations. The applied stress intensities were ±5 MPa, ±10 MPa, ±15 MPa, and ±20 MPa (+ for tensile and - for compression stresses). The imposed magnetic induction waveform is sinusoidal with amplitudes ranging from 0.05 T to 1.5 T with 0.05 T steps. This represents more than 780 measurements made at this stage of experimental data acquisition.

To set the mechanical stress imposed on the sample, it is necessary to adjust the displacement parameter of the MECMESIN® equipment to reach the force equivalent to the desired stress. Once the mechanical part of the setup is configured, the magnetization of the sample must be set up. To do so, the control bench must be turned on. At each test, the sample is demagnetized, and the desired operating points are adjusted by modifying the reference of the signal sent to the control for obtaining a voltage value induced in the secondary winding equivalent to the desired magnetic induction. The voltage signals from the sensors undergo a filtering/amplification stage and after the adjustment process, the signals are acquired.

B. Measurements

The magnetic induction $B(t)$ on the sheets under test are obtained by integrating the voltage induced in the secondary winding of the SST knowing the cross-sectional area of the sample and the winding number of turns.

The magnetic field $H(t)$ at the surface of the sheet is evaluated based on the extrapolation of the magnetic field measured by three H-coils sensors located at different known positions from the sample and inserted in the anti-buckling fixture [5].

Once $B(t)$ and $H(t)$ are known, the magnetic losses are evaluated by (1), where ρ is the material density [kg/m³].

$$W = \frac{1}{\rho} \oint H(t)dB \quad [J/kg] \tag{1}$$

The material losses are measured at 1 Hz for three angles between lamination and cutting directions and at all applied load levels. Fig. 2 shows the hysteresis loops at 1 T for the three angles between lamination and cutting directions where one observes an expressive increase of the loop surfaces for compressive stresses while a small reduction of the loops for tensile ones. Fig. 2 (a) and Fig. 2 (b) depict loops under tension and compression for sample RD, while the pairs comprising Fig. 2 (c) and Fig. (d) as well as Fig. 2 (e) and Fig. (f) represent the same for sample DD and TD, respectively. Similar behavior is observed in the hysteresis losses shown in Fig. 3 (a), Fig. 3 (b) and Fig. 3(c) for the samples RD, DD and TD, respectively.
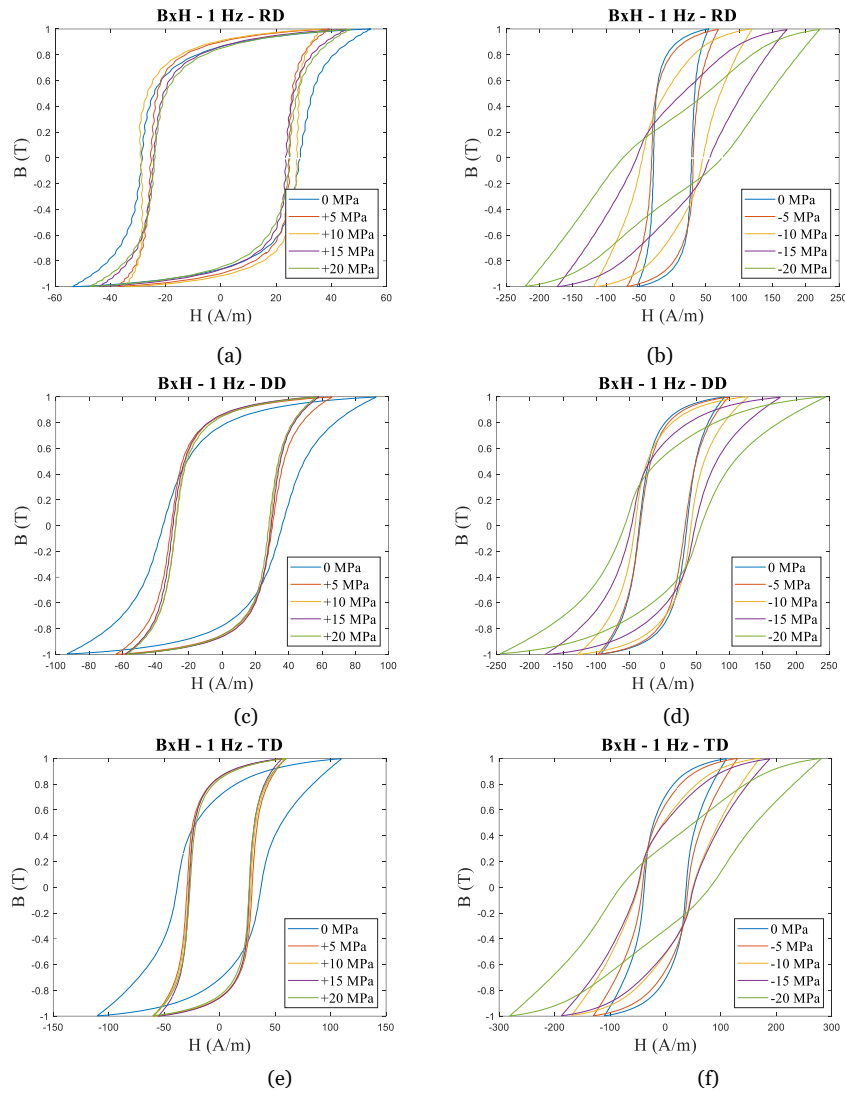
Fig. 2. Hysteresis loops at 1 T and for the sample RD with (a) tensile and (b) compressive stresses; sample DD with (c) tensile and compressive stress and for the sample TD with (e) tensile and (f) compressive stress.
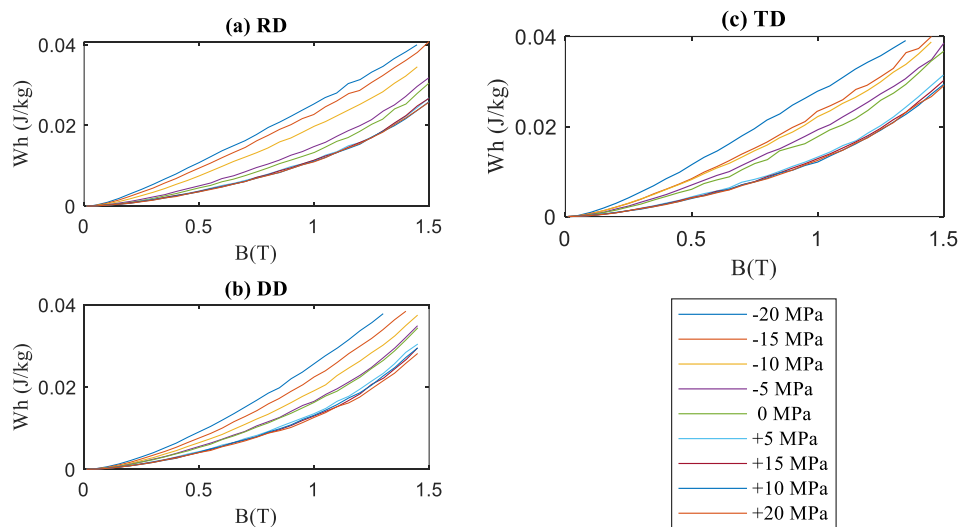

Fig. 3. Hysteresis losses as a function of magnetic induction at different levels of mechanical stress for (a) RD, (b) DD and (c) TD samples.

III. RESULTS AND DISCUSSION

Widely discussed studies in the literature determine three distinct components for iron losses: hysteresis, eddy current and excess losses. Among these three types of losses, it is known that the losses that undergo the most significant changes in their values due to mechanical stresses are hysteresis losses W_h. Therefore, parameters of six different models representing hysteresis losses are analyzed.

All the models represent hysteresis losses in [J/kg] and were analyzed by the relative percentage differences among loss values estimated by the models (for each peak magnetic induction value) and the experimentally ones, as well as the coefficient of determination R^2 value [6] for each loss model curve. Table I summarizes the six methods used to represent hysteresis losses (W_{h_1} to W_{h_6}). where B_p is the peak of the magnetic induction (other parameters are constants determined by curve fitting).

For the six hysteresis models presented in Table I the parameter values were obtained for all the levels of mechanical stresses through curve fitting optimization using Generalized Reduced Gradient (GRG) [7]. The sixth-order polynomial model (model 6) presented the coefficient of determination R^2 closest to 1 for all three samples. However, as a relatively high-order polynomial model, it easily fits the curve shape but exhibits significant variation on parameter values, resulting in a trade-off when using it to represent hysteresis losses. Although this model provides a good representation of experimental data, it does not offer a homogeneous behavior of the parameter values with respect to the applied loading. Therefore, the sixth-order polynomial model (model 6) is not the most suitable. Among the analyzed models, the method that presented the highest R^2 values (after the sixth-order polynomial model) was model 4, a variation of the Steinmetz model. The dots in Fig. 4 show the behavior of K_{h_4}, α_{0_4} and α_{3_4} parameters of the selected hysteresis model for the three different samples. It should be noted that the remaining α_{1_4} and α_{2_4} parameters are null.

TABLE I: HYSTERESIS LOSSES MODELS

Model	Formulation	References
1	$W_{h_1} = K_{h_1} B_p^{\alpha_{01}}$	[8]
2	$W_{h_2} = K_{h_2} B_p^{\alpha_{02} + \alpha_{12} B_p}$	[9]
3	$W_{h_3} = K_{h_3} B_p^{\alpha_{03} + \alpha_{13} B_p + \alpha_{23} B_p^2}$	[10]
4	$W_{h_4} = K_{h_4} B_p^{\alpha_{04} + \alpha_{14} B_p + \alpha_{24} B_p^2 + \alpha_{34} B_p^3}$	[11]
5	$W_{h_5} = x_{1_5} B_p + x_{2_5} B_p^2$	[12]
6	$W_{h_6} = x_{0_6} + x_{1_6} B_p + x_{2_6} B_p^2 + x_{3_6} B_p^3$ $+ x_{4_6} B_p^4 + x_{5_6} B_p^5 + x_{6_6} B_p^6$	[13]

The hysteresis loss model parameters values obtained in the performed tests are determined at specific stress levels. However, it is desirable to obtain a function that allows estimating the loss parameter values for any mechanical stress, since it is necessary to predict the behavior of hysteresis losses when the material is subjected to mechanical stresses σ of any intensity (within or close to the measurement

range of ±20 MPa). Based on the values of the chosen model parameters, the average of the values is initially calculated to obtain a function that can be used independently of the lamination direction. Knowing the values within the measurement range, as well as the trend of parameter behavior under stresses beyond the ±20 MPa range, a generic function $g_k(\sigma)$, obtained by a curve fitting procedure, is empirically proposed according to (2). In this equation c_0 to c_6 are constants while $g_1(\sigma)$ interpolates K_{h_4} and $g_2(\sigma)$ and $g_3(\sigma)$ do it respectively to α_{0_4} and α_{3_4}. Still in (2), the sign before the second term in the right side is positive for $g_1(\sigma)$ while it is negative for $g_2(\sigma)$ and $g_3(\sigma)$.

$$g_k(\sigma) = c_0\tan^{-1}[c_1\sigma + c_2] \pm c_3\tan^{-1}[c_4\sigma - c_5] + c_6 \qquad (2)$$

Table II presents the corresponding parameters obtained by means of function *curve_fit* of scientific library scipy [14]. The resulting coefficient of determination R^2 are also given in the same Table II and one observes that, as they are close to 1.0, the curve fitting is satisfactory achieved.

TABLE II: INTERPOLATION FUNCTION $g_k(\sigma)$

Parameter	$g_k(\sigma)$		
	K_{h_4}	α_{0_4}	α_{3_4}
c_0	-0.0799	7.0457	0.1010
c_1	0.1645	0.1353	0.0863
c_2	2.0046	2.1080	0.5571
c_3	-0.0723	6.7549	0.0216
c_4	-0.1757	0.1400	0.3961
c_{05}	2.1370	-2.1605	5.4053
c_6	0.0215	1.2905	0.0537
R^2	0.9915	0.9960	0.9892

Fig. 4 shows the behavior of the proposed function (2) for the parameters K_{h_4} (Fig. 4 (a)) , α_{0_4} (Fig. 4 (b)) and α_{3_4} (Fig. 4 (c)) in the continuous black curve. In the same figure are the experimental values of the parameters for the RD, DD, and TD samples are represented in blue, red and green respectively, as well as the average values of these parameters for the three samples shown as black crosses.
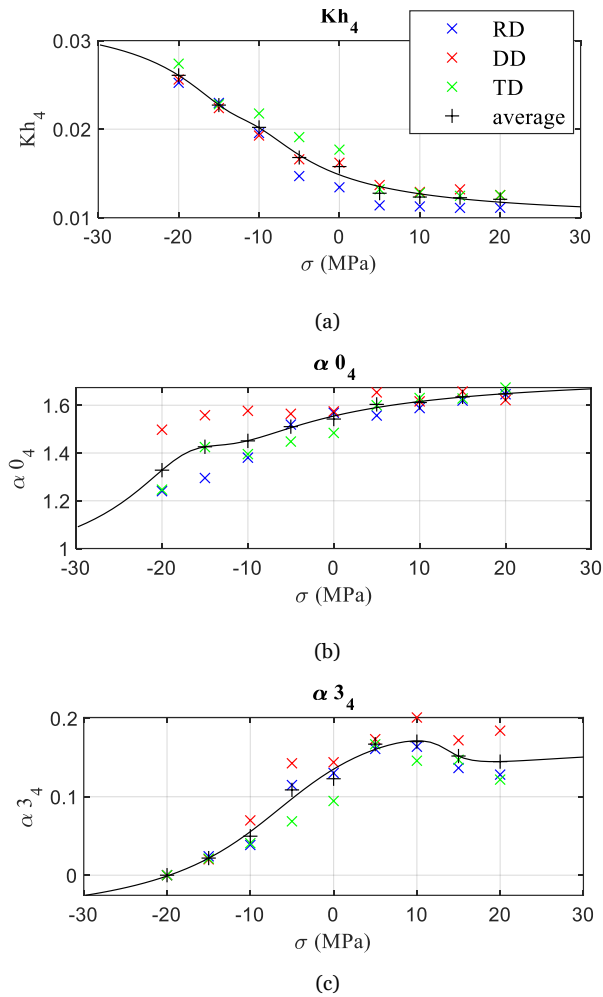
Fig. 4. Curve fitting from experimental results for: (a) K_{h_4}; (b) α_{0_4} and (c) α_{3_4}.

Knowing the behavior of the hysteresis losses as a function of stress, the parameters of the model are adjusted according to the local equivalent stress to perform the magneto-mechanical coupling.

A. *Losses in an Electrical Machine Stator*

The chosen study device is a single-phase induction motor stator. The magnetic excitation of the stator is composed by two windings fed by two 90° shifted voltages placed on a magnetic head occupying the place of the rotor of the original motor (Fig. 5) [16]. Such topology allows the application of mechanical loadings on the stator external surface.

Fig. 5. Magnetic head used for exciting the unwounded stator sample.

Simulations were carried out using a compressive stress of 7.5 MPa applied uniformly on the left and right sides of the half stator domain shown in Fig. 6 presenting also the FE mesh used in calculations.

A mechanical FE stress distribution calculation is initially performed in order to obtain a stress tensor over the calculation domain. With such a tensor and the magnetic field calculated by electromagnetic FE method using the same mesh, an equivalent stress distribution can be obtained for taking into account the multiaxial mechanical stresses in the device, as given by (3), where s is the deviatoric part of the stress, h is the unit vector on the direction of the magnetic field and h^t is h transposed [15].

$$\sigma_{eq} = \frac{3}{2} h^t \cdot s \cdot h \tag{3}$$
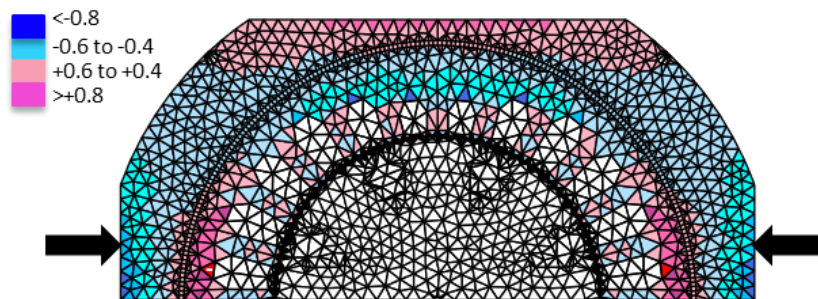

Fig. 6. Distribution of the normalized equivalent stresses with the scale given in pu using the maximum absolute value as the base.

The calculated distribution of the normalized equivalent stress is also shown in Fig. 6. In this figure, the scale is given in pu using the maximum absolute value as the base. One observes that locally there are compression but also traction stresses. The region close to the surface where the forces are applied presents a higher concentration of local (negative sign) compression efforts, in coherence with the nature of the applied load. Overall, there is a predominance of equivalent compression efforts, which indicates, as one can observes in Fig.3, that an increase in hysteresis losses should be observed.

The approximation given in (4) is chosen to calculate the hysteresis loss W_{h_4} in the numerical simulations by FE method, where B_p is the peak of magnetic induction and other parameters are given by (2) (or from the continuous lines of Fig. 3).

$$W_{h_4} = K_{h_4} B_p^{\alpha_{0_4} + \alpha_{3_4} B_p^3} \tag{4}$$

Simulation results presented an increase in hysteresis losses of about 16% when compared with the stressless case (calculated with (4) for K_{h_4}, α_{0_4} and α_{3_4} parameters at null stress value). On Fig. 7, a graphical view of the distribution of hysteresis losses difference between the two cases, with the measurements of the differences given in percentage, can be observed.
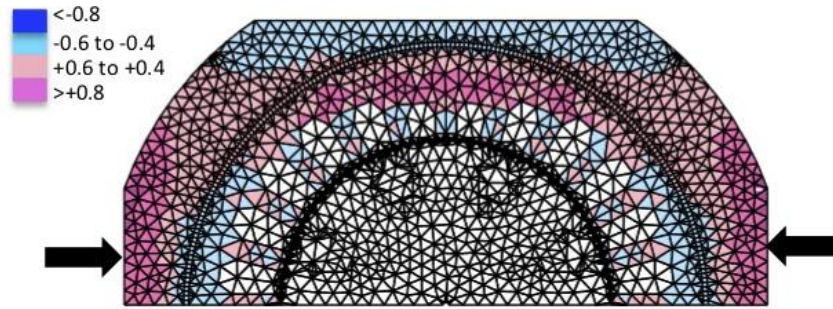

Fig. 7. Distribution of the relative percent difference in hysteresis losses in comparison between stressless and stress conditions.

As Fig. 6 shows compression and traction equivalent stresses, it is coherent that in Fig. 7 positive differences (increase of losses) as well as negative differences (reduction of losses) between stressless and stress conditions occur. In fact, Fig. 7 is expected to be a "dual" distribution related to the behavior of Fig. 6, where for every shade of blue in one figure, there will be a red shade in the other and vice versa.

IV. CONCLUSIONS

This research provides a hysteresis losses calculation formulation considering mechanical efforts. Several experimental data for an electrical silicon steel were obtained and processed in order to obtain an effective model. A generic equation form is used to obtain the evolution of the model parameters according to stress values. In such a way, researchers can easily use them and the data provided in the paper when evaluating hysteresis losses under mechanical loadings for other machines and electromagnetic devices.

The simulations performed highlight the complexity of magneto-mechanical coupling on real devices. For a compressive mechanical load applied on the stator, an increase in hysteresis losses has been verified. The proposed setup and methodology offer a convenient way to estimate a posteriori loss evaluation accounting for stress on macro structure under controlled condition.

REFERENCES

[1]   L. Bernard and L. Daniel, "Effect of stress on magnetic hysteresis losses in a switched reluctance motor: Application to stator and rotor shrink fitting," *IEEE Transactions on Magnetics*, vol. 51, 2015, doi: 10.1109/TMAG.2015.2435701.
[2]   J. Karthaus, S. Steentjes, and K. Hameyer, "Mechanical stress-dependency of iron losses in non-oriented electrical steel sheets," *XXIV Symposium Electromagnetic Phenomena In Nonlinear Circuits*, pp. 111–112, 2016.

[3] U. Aydin *et al.*, "Effect of multi-axial stress on iron losses of electrical steel sheets," *Journal of Magnetism and Magnetic Materials*, vol. 469, pp. 19–27, 2019, doi: 10.1016/j.jmmm.2018.08.003.

[4] B. J. Mailhé *et al.*, "Modified-SST for Uniaxial Characterization of Electrical Steel Sheets Under Controlled Induced Voltage and Constant Stress," *IEEE Transactions on Instrumentation and Measurement*, vol. 69, no. 12, pp. 9756–9765, 2020.

[5] B. J. Mailhé *et al.*, "Influence of shielding on the magnetic field measurement by direct H-coil method in a double-yoked SST," *IEEE Transactions on Magnetics*, vol. 54, no. 3, 2018, doi: 10.1109/TMAG.2017.2758959.

[6] C. Lewis-Beck and M. Lewis-Beck, "Applied regression: An introduction". Sage publications, 2015.

[7] L. S. Lasdon, A. D. Waren, A. Jain, and M. Ratner, "Design and Testing of a Generalized Reduced Gradient Code for Nonlinear Programming," *ACM Transactions on Math*ematical *Software,* vol. 4, no. 1, pp. 34–50, 1978, doi: 10.1145/355769.355773.

[8] C. P. Steinmetz, "On the law of hysteresis", *Proceedings of the IEEE*, vol.72, 1984, doi: 10.1109/PROC.1984.12842.

[9] M. I. Miller, T. J. E.; McGilp, "PC-BDC 6.5 for Windows-Software." SPEED Laboratory, University of Glasgow, 2004.

[10] Y. Chen and P. Pillay, "An improved formula for lamination core loss calculations in machines operating with high frequency and high flux density excitation", *IEEE Industry Applications Society*, vol. 2, pp. 759–766, 2002, doi: 10.1109/IAS.2002.1042645.

[11] D. M. Ionel *et al.*, "On the variation with flux and frequency of the core loss coefficients in electrical machines," *IEEE Transactions on Industry Application*, vol. 42, no. 3, pp. 658–667, 2006, doi: 10.1109/TIA.2006.872941.

[12] N. J. Batistela, Characterization and electromagnetic modeling of Silicon-steel sheets, PhD Dissertation, University Federal of Santa Catarina, 2001.

[13] B. J. Mailhé, Characterization and modelling of the magnetic behaviour of electrical steel under mechanical, PhD Dissertation, University Federal of Santa Catarina, 2018.

[14] "SciPy.org." https://docs.scipy.org/doc/. Accessed May 01, 2023.

[15] L. Daniel and O. Hubert, "An equivalent stress for the influence of multiaxial stress on the magnetic behavior," *Journal of Applied Physics*, vol. 105, no. 7, 2009, doi: 10.1063/1.3068646.

[16] J. P. Schlegel, et al., "Core tester iron losses segregation by finite element modeling," *IEEE Transactions on Magnetics*, vol. 48, no. 2, pp. 715–718, 2012, doi: 10.1109/TMAG.2011.2172777.